Journal of Carcinogenesis
Covering Genesis to Therapeutics

Journal of Carcinogenesis, ISSN: 1477-3163
2024; Vol 23: Issue 1, https://carcinogenesis.com/

Evaluation of Curcumin and Dimethyl Chalcone in Neuropathic Pain Management Insights from In-Vivo Chronic Constriction Injury Model and Histological Analysis.

Swathi Vutkuri[1], Shabna Roupal Morais[*2], Sailendra Kumar Mahanta*[3], Sisir nandi[4], Chandru R[5], Latha S[6]

[1]Research Scholar, Sri Ramachandra Faculty of Pharmacy, SRIHER(DU), Porur, Chennai India & Department of Pharmacology, Narasaraopeta Institute of Pharmaceutical Sciences, Narasaraopeta, India.

[2]Associate Professor, Department of Pharmacognosy, Sri Ramachandra Faculty of Pharmacy, SRIHER(DU), Porur, Chennai.

[3]Department of Pharmacology, School of Pharmacy, The Assam Kaziranga University, India.

[4]Department of Pharmaceutical Chemistry, Global Institute of Higher Education and Research, Chennai, India.

[5]Department of General Surgery, Sri Ramachandra Institute of Higher Education and Research, Chennai, India.

[6]Former Assistant Professor, Department of Pharmacognosy, Sri Ramachandra Faculty of Pharmacy, SRIHER(DU), Porur, Chennai.

Corresponding author*

Shabna Roupal Morais,

Email ID : shabnaroupal@sriramachnadra.edu.in

Co-Corresponding author:

Sailendra Kumar Mahanta,

Email ID : sailendra04@gmail.com & sailendrakumar@kzu.ac.in

ABSTRACT

The transient receptor potential ankyrin 1 (TRPA1) receptor plays a pivotal role in various physiological processes, notably in the sensory transduction of pain and inflammation. By responding to a myriad of stimuli, including environmental irritants and endogenous inflammatory mediators, TRPA1 influences the sensation of pain. This receptors activation is crucial in pathophysiological conditions such as asthma, arthritis, and neuropathic pain, where heightened TRPA1 sensitivity often correlates with increased symptom severity. Recent research highlights the potential of targeting TRPA1 in therapeutic applications, offering a promising avenue for alleviating chronic pain and inflammatory disorders. Pharmacological agents designed to modulate TRPA1 activity could provide innovative treatment options, bridging the gap between traditional pain management and modern medicine. As scientists continue to unravel TRPA1s multifaceted roles, a clearer understanding of its mechanisms could lead to the development of more effective and safer therapies, ultimately enhancing patient care in various health contexts. This study explores the interactions of (E)-3-(4- (dimethylamino)phenyl)-1-(2,4-dimethylphenyl)prop-2-en-1-one, curcumin, and its metabolites with the TRPA1 receptor, highlighting their potential as therapeutic agents for the treatment of neuropathic pain.

Keywords: *TRPA1, curcumin, (E)-3-(4-(dimethylamino)phenyl)1(2,4dimethylphenyl)prop-2-en-1-one, Neuropathic pain*

How to Cite: Swathi Vutkuri, Shabna Roupal Morais, Sailendra Kumar Mahanta, Sisir nandi, Chandru R, Latha S, (2024) Evaluation of Curcumin and Dimethyl Chalcone in Neuropathic Pain Management Insights from In-Vivo Chronic Constriction Injury Model and Histological Analysis., *Journal of Carcinogenesis*, *Vol.23, No.1*, 216-234.

1. INTRODUCTION

The exploration of TRPA1 receptors unveils their crucial role in sensory perception and pain pathways. These receptors, part of the transient receptor potential (TRP) family, function as sensors for various environmental stimuli, including temperature changes, irritants, and inflammatory mediators. Their activation triggers a cascade of physiological responses that can lead to sensations commonly associated with pain and discomfort, highlighting their significance in nociception...

Understanding the mechanisms by which TRPA1 receptors operate not only enhances our knowledge of basic sensory biology but also opens potential avenues for therapeutic interventions in pain management and treatment of related disorders. The implications of TRPA1 function extend beyond simple pain perception, influencing a broad spectrum of physiological processes, thus marking them as pivotal components in both health and disease. In the ensuing sections, the current research will delve deeper into the molecular structure, activation modalities, and potential therapeutic targets associated with TRPA1 receptors

Overview of TRPA1 receptor and its significance in sensory biology

Integral to our understanding of sensory biology, the TRPA1 receptor functions as a pivotal sensor for noxious stimuli, contributing significantly to pain perception and nociception across various organisms. Its activation is often triggered by environmental irritants, leading to a cascade of biological responses that ultimately result in protective behaviours. For instance, in planarians, TRPA1 is crucial for inducing scrunching a stereotypical escape mechanism in response to harmful agents like heat and certain chemicals. This receptor's ability to integrate multiple sensory signals underscores its role in adaptive responses, highlighting not just a pathway of sensation but a convergence point where various stimuli elicit similar protective reactions. Furthermore, research on TRPA1 in zebrafish demonstrates its relevance beyond merely the perception of pain; the genes manipulation can alter chronic pain behaviors, illustrating its significance across species in understanding pain signaling mechanisms (1).

Structure and Function of TRPA1 Receptor

In exploring the structure of the TRPA1 receptor, it becomes clear how its unique configuration facilitates a diverse range of physiological functions, particularly in sensory perception. TRPA1, a member of the transient receptor potential (TRP) channel superfamily, is characterized by its distinct pore-forming region, which allows ions such as calcium and sodium to flow into the cell upon activation. This ion influx is essential for various cellular processes, including pain sensation and inflammatory responses.[1] One critical function of TRPA1 is its role in nociception, as it responds to noxious stimuli like heat and irritants, activating pathways that can lead to reflexive protective behaviours, such as scrunching in planarians. This suggests that TRPA1 not only serves as a sensory transducer but also contributes significantly to behavioural responses, emphasizing the receptors evolutionary importance in survival mechanisms. The multifaceted role of TRPA1 underscores its potential as a therapeutic target for pain management and other sensory disorders (1, 2).

Molecular characteristics and physiological roles of TRPA1

The TRPA1 receptor, a member of the transient receptor potential (TRP) channel family, exhibits distinct molecular characteristics that enable its wide-ranging physiological roles. This receptor is activated by various stimuli, including environmental toxins and endogenous compounds, leading to its involvement in nociception and thermal sensation. Notably, TRPA1 is crucial for the detection of painful stimuli, as highlighted by its activation in response to noxious conditions such as extreme pH and temperature, which may evoke defensive behaviours like scrunching in planarians. The physiological significance of TRPA1 extends beyond pain perception; it is also implicated in metabolic regulation, where estrogen metabolites enhance pancreatic β-cell function through TRPA1 activity, promoting insulin secretion in response to glucose stimulation. Thus, TRPA1 serves as a pivotal molecular mediator, linking environmental stimuli to vital physiological processes in both sensory and metabolic systems (3, 4).

TRPA1 Receptor in Pain and Inflammation

The TRPA1 receptor plays a crucial role in mediating pain and inflammation, particularly in response to various noxious stimuli. This ion channel is expressed in sensory neurons and becomes activated by inflammatory mediators released following tissue injury or infection. Activation of TRPA1 contributes to the sensation of hyperalgesia, as it intensifies pain signalling pathways within the nervous system. As noted in previous studies, prolonged inflammation can provoke the release of factors that sensitize TRPA1, further exacerbating pain responses . Additionally, the interplay between TRPA1 and innate immune pathways highlights its function as a critical mediator in the inflammatory process (5). Understanding the mechanisms underlying TRPA1 receptor activation could lead to novel therapeutic approaches aimed at mitigating chronic pain conditions associated with unresolved inflammation and enhancing overall patient care (6, 7). Thus, TRPA1 remains a focal point for research in the context of pain modulation and inflammation.

Mechanisms of TRPA1 activation in nociception and inflammatory responses

Understanding the activation mechanisms of TRPA1 is crucial for unravelling its role in nociception and inflammatory responses. TRPA1 channels act as sensors for various noxious stimuli, including extreme temperatures and harmful chemicals, making them vital for detecting pain (8). When activated by these stimuli, TRPA1 channels facilitate the influx of cations, leading to neuronal depolarization and the transmission of pain signals. Moreover, the expression of different TRPA1 isoforms can significantly influence nociceptive response specifically, the TrpA1(E) isoform has been shown to

inhibit thermal responses in other isoforms, indicating a complex regulatory mechanism at play (9). Furthermore, the interaction of TRPA1 with various binding partners through mechanisms such as co-immunoprecipitation suggests that TRPA1s functionality is not only dependent on its intrinsic properties but also on its extracellular environment. This interplay of factors underlines TRPA1s importance in pain modulation and potential therapeutic targets for chronic inflammatory conditions (4).

The investigation into the TRPA1 receptor underscores its pivotal role in sensory transduction and its modulation by inflammatory processes. Additionally, the electrical conductance properties observed in TRP channels demonstrate that lipid membranes can mimic certain channel behaviours, suggesting that investigations of synthetic lipid bilayers can further illuminate ion channel activities (10). Thus, a comprehensive understanding of TRPA1 dynamics presents opportunities for novel approaches in treating pain and inflammation. This research investigates the interactions of (E)-3-(4-(dimethylamino)phenyl)-1-(2,4-dimethylphenyl)prop-2-en-1-one, curcumin, and its metabolites with the TRPA1 receptor as a potential therapeutic strategy for managing neuropathic pain.

2. METHODOLOGY

Molecular Docking of Curcumin, its derivatives and (E)-3-(4-(dimethylamino)phenyl)-1-(2,4-dimethylphenyl)prop-2-en-1-one with TRPA1 receptor

The molecular docking study was conducted using the Dock Ligands (CDOCKER) protocol, an implementation of the CDOCKER algorithm, which is a grid-based molecular docking method employing the CHARMm force field (11). In this approach, the receptor structure was kept rigid while the ligand molecules were allowed to adopt flexible conformations during refinement. The protocol was initiated by preparing the receptor structure, ensuring the addition of hydrogen atoms and proper valency satisfaction for accurate atomic typing. Binding site spheres were defined using the Define and Edit Binding Site tool, allowing for precise ligand placement within the active site. Ligand preparation involved the addition of hydrogen atoms and the satisfaction of valency requirements to ensure compatibility with the docking process. Ligands were either positioned near the receptor cavity or assigned to an Input Site Sphere if not pre-docked. The docking process began with the generation of random ligand conformations through high-temperature molecular dynamics, followed by random rotations to explore diverse orientations. These conformations were then subjected to simulated annealing, utilizing a grid-based refinement (GRID 1), and further optimized through either grid-based or full force field minimization. It is noteworthy that the high-temperature molecular dynamics step had the potential to alter ligand stereochemistry, including cis-trans isomerization. The docking calculations were executed using the Dock Ligands (CDOCKER) tool within the Receptor-Ligand Interactions module. Key parameters, such as input receptor, input ligands, and input site sphere, were set accordingly. Additional protocol parameters were adjusted as needed, including the number of generated random conformations and orientations. For a simplified refinement process without generating new ligand conformations, the parameters for Random Conformations and Orientations to Refine were set to zero.

Upon execution, the docking job's status was monitored through the Discovery Studio interface, with an option to send the job to the background for continued workflow efficiency. The output consisted of a set of refined ligand poses, which were analyzed for receptor-ligand interactions within the Molecule Window. The results provided insights into the binding affinities and conformational preferences of the docked ligands within the receptor’s active site (11).

Binding Site Analysis using Discovery Studio Visualizer

Binding site analysis is crucial for understanding the interaction of Curcumin, its derivatives, and (E)-3-(4-(dimethylamino)phenyl)-1-(2,4-dimethylphenyl)prop-2-en-1-one with the TRPA1 (6X2J) protein. This study is conducted using BIOVIA Discovery Studio Visualizer, which helps identify potential binding pockets and analyze molecular interactions. The first step involves loading the protein structure by importing the PDB file of TRPA1 (6X2J) into Discovery Studio. Water molecules and unwanted heteroatoms are removed to ensure a clean structure for analysis (12).

Once the protein is prepared, the binding site is identified using the find Sites from Receptor Cavities tool. Discovery Studio predicts possible binding pockets based on cavity volume and accessibility. The most relevant binding pocket is selected based on its proximity to known active sites. Next, the ligand molecules, including Curcumin, its derivatives, and the chalcone derivative, are prepared. These molecules are imported in SDF, MOL, or PDB format, and their geometries are optimized using the Minimize Energy function under the Prepare Ligands section. This ensures that the ligands are in their most stable conformations for interaction analysis.

To analyze ligand-protein interactions, the protein and ligand are selected from the Molecule Explorer panel, followed by choosing Analyze Ligand Interactions. Discovery Studio visualizes hydrogen bonding, hydrophobic interactions, and π-stacking interactions between the ligands and the binding site residues. A 2D interaction diagram and 3D visualization are generated, allowing for a detailed examination of molecular interactions.

The binding interactions are evaluated by identifying key interacting residues and measuring hydrogen bond distances, hydrophobic forces, and electrostatic interactions. The software provides an interaction table summarizing these findings. Additionally, the binding energy and affinity are assessed to determine the strength of interactions between the ligands and

TRPA1. Finally, the results are saved by exporting the 2D interaction diagrams, binding site cavity details, and molecular interaction images in various formats, such as PNG. The binding site analysis helps to determine the most favourable binding site and interaction patterns, providing valuable insights for molecular docking studies, binding energy calculations, and lead optimization in drug discovery.

MD Simulations for the protein and ligand structures

Molecular dynamics (MD) simulation was conducted to analyze the interaction of Curcumin, its derivatives, and (E)-3-(4-(dimethylamino)phenyl)-1-(2,4-dimethylphenyl)prop-2-en-1-one with the TRPA1 (6X2J) protein using the GROMACS software package. This simulation technique applies Newton's laws of motion to study atomic movements within the protein-ligand complex. The first step involved energy minimization of the protein-ligand complex in vacuum using the steepest descent algorithm, which iteratively optimized the atomic coordinates to achieve the lowest potential energy. Following minimization, the complex was solvated in a periodic water box using the SPC (Simple Point Charge) water model, ensuring a realistic aqueous environment for the simulation. To mimic physiological conditions, a 0.15 M salt concentration was maintained by adding sodium (Na^+) and chloride (Cl^-) ions to the system. The system was then subjected to NPT (constant pressure, constant temperature) equilibration, stabilizing the complex under biologically relevant conditions. This was followed by the production run, which was performed for 100 ns and 300 ns under the NPT ensemble to observe the dynamic behavior of the protein-ligand complex over time.

After the simulation, trajectory analysis was conducted using various GROMACS tools to examine structural stability and ligand interactions. Key analyses included Root Mean Square Deviation (RMSD) to assess the overall stability of the complex, Root Mean Square Fluctuation (RMSF) to study the flexibility of protein residues, Radius of Gyration (Rg) to measure the compactness of the structure, Solvent Accessible Surface Area (SASA) to evaluate solvent exposure, and Hydrogen Bonding (H-Bond) analysis to investigate interactions between the ligand and protein. These evaluations provided insights into the conformational changes and binding dynamics of the ligands with TRPA1.

Additionally, Molecular Mechanics Poisson–Boltzmann Surface Area (MMPBSA) calculations were performed to quantify the binding free energy of each ligand with TRPA1. The last 50 ns of the GROMACS trajectories were extracted for MMPBSA analysis. The complex structures were first prepared, including explicit solvent addition and topology generation, followed by energy decomposition using the MMPBSA method. This analysis determined the binding affinity and the contributions of various energy components to the overall binding interaction. The findings from MMPBSA calculations would help in identifying the most stable ligand conformations, key binding sites, and critical interactions responsible for the binding of Curcumin and its derivatives to TRPA1 (6X2J) (13, 14).

In-vivo Chronic Constriction Injury animal model for neuropathic pain for evaluating Curcumin, its derivatives, and (E)-3-(4-(dimethylamino)phenyl)-1-(2,4-dimethylphenyl)prop-2-en-1-one

The Chronic Constriction Injury (CCI) model was employed to induce neuropathic pain in small animals, following ethical guidelines for animal research. Male S.D. rats weighing 150 gm were housed under standard conditions with ad libitum access to food and water and anesthetized using isoflurane (inhalation) (15). A 1.5 cm incision was made 0.5 cm below the pelvis along the posterior thigh, and the biceps femoris and gluteus superficialis muscles were carefully separated to expose and isolate the sciatic nerve. Four loose ligatures of 5–0 chromic catgut were placed around the sciatic nerve at 1 mm intervals, ensuring partial constriction without completely occluding nerve conduction. The chromic catgut material also contributed to an inflammatory response, further exacerbating neuropathic pain symptoms. Following ligation, the muscles were repositioned, and the incision was closed using absorbable sutures or surgical staples. Pain behaviour (Paw pressure Test) was assessed on the 10^{th} day post-surgery using Randall Sellitto at 3hr post dosing of curcumin and chalcone derivative. Percentage reversal of hyperalgesia was estimated using the following formula:

$$\% \text{ Reversal} = \frac{\text{Ipsilatral post dose} - \text{Ipsilatral pre dose}}{\text{Contra latral pre dose} - \text{Ipisilatral pre dose}} * 100\%$$

Histological Analysis of Sciatic nerve samples

Following euthanasia, the ipsilateral sciatic nerve from animals subjected to Chronic Constriction Injury (CCI) was carefully dissected. The nerve samples were immediately fixed in 10% neutral buffered formalin (NBF) for 24–48 hours at room temperature to preserve tissue morphology and prevent autolysis.

After fixation, the nerve tissues underwent a dehydration process using a graded ethanol series (70%, 80%, 95%, and 100%) followed by xylene clearing to remove residual alcohol. The samples were then embedded in paraffin wax to facilitate sectioning. Longitudinal sections (LS) of the ipsilateral sciatic nerve were prepared using a microtome, with sections cut at 4–6 µm thickness. The sections were then mounted on glass slides and dried at 60°C for 30 minutes to ensure proper adhesion before staining.

For Hematoxylin and Eosin (H&E) staining, the paraffin-embedded nerve sections were deparaffinized in xylene (2 × 5

min) and gradually rehydrated through an ethanol gradient (100%, 95%, 80%, 70%) before being rinsed in distilled water. The sections were then immersed in Hematoxylin for 5 minutes, followed by rinsing in running tap water until the nuclei appeared blue. Differentiation was performed using 1% acid alcohol for a few seconds, followed by bluing in 0.2% ammonia water for 30 seconds. Subsequently, the sections were counterstained with Eosin for 2 minutes, washed in distilled water, and dehydrated through an ascending ethanol series (70%, 80%, 95%, and 100%), followed by xylene clearing (2 × 5 min). The stained sections were mounted using DPX mounting medium and covered with a glass coverslip. The prepared slides were examined under a light microscope at various magnifications to assess nerve morphology, axonal degeneration, myelin sheath integrity, inflammatory cell infiltration, and fibrosis. Images were captured for qualitative and quantitative analysis. This histological evaluation of sciatic nerve provided critical insights into CCI-induced nerve damage, including structural alterations, inflammatory responses, and degenerative changes in the sciatic nerve post-injury (16).

3. RESULTS AND DISCUSSION

Molecular Docking and Binding Site Analysis

The docking results presented in Fig.1 illustrate the interaction between curcumin and a target protein, as analyzed using the CDOCKER protocol. The left section of the image shows the 3D representation of the protein-ligand complex, where the protein is depicted in a ribbon model with different colors representing different secondary structural elements. Curcumin is shown as a stick model within the binding pocket of the receptor. The inset magnifies the interaction region, highlighting the ligand binding mode.

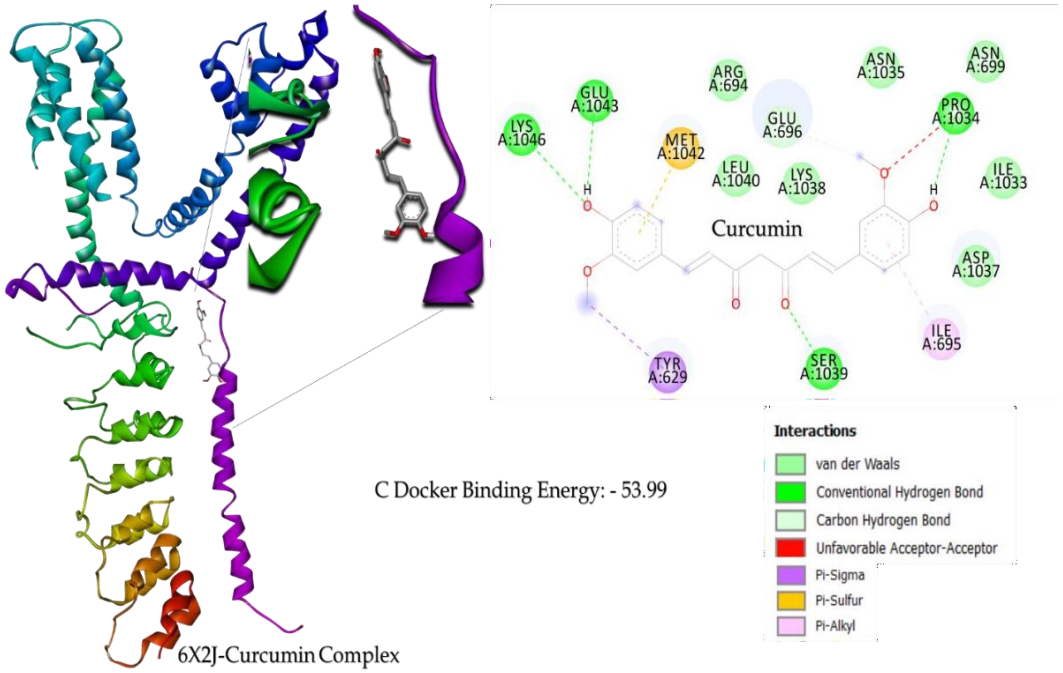

Figure 1: Binding Energy and 2D Binding site analysis of 6X2J and Curcumin complex

The right section of the image provides a 2D interaction map of curcumin within the active site, detailing specific intermolecular interactions with surrounding amino acids. Several residues, including LEU A:1040, GLU A:1043, ILE A:1033, and ASN A:1035, engage in non-covalent van der Waals interactions, contributing to ligand stabilization within the pocket. Curcumin forms hydrogen bonds with LYS A:1038 and SER A:1039, which play a crucial role in stabilizing the ligand and enhancing binding affinity. Residues like MET A:1042 contribute via weak carbon hydrogen bonding, aiding in ligand positioning.

A potential electrostatic clash is observed, suggesting a repulsive interaction that might slightly affect binding efficiency. Curcumin interacts with TYR A:629 (Pi-Sigma, Purple) and MET A:1042 (Pi-Sulfur, Yellow), indicating aromatic stacking and hydrophobic contributions that enhance ligand affinity. Additional hydrophobic interactions with ILE A:695 provide further stabilization.

The docking study suggests that curcumin binds effectively within the receptor's active site, forming multiple stabilizing interactions, particularly hydrogen bonds and van der Waals forces. The presence of Pi-Sigma and Pi-Alkyl interactions implies that curcumin's aromatic rings contribute significantly to its binding affinity. The unfavourable acceptor-acceptor interaction might indicate an area for structural modification of curcumin to optimize binding.

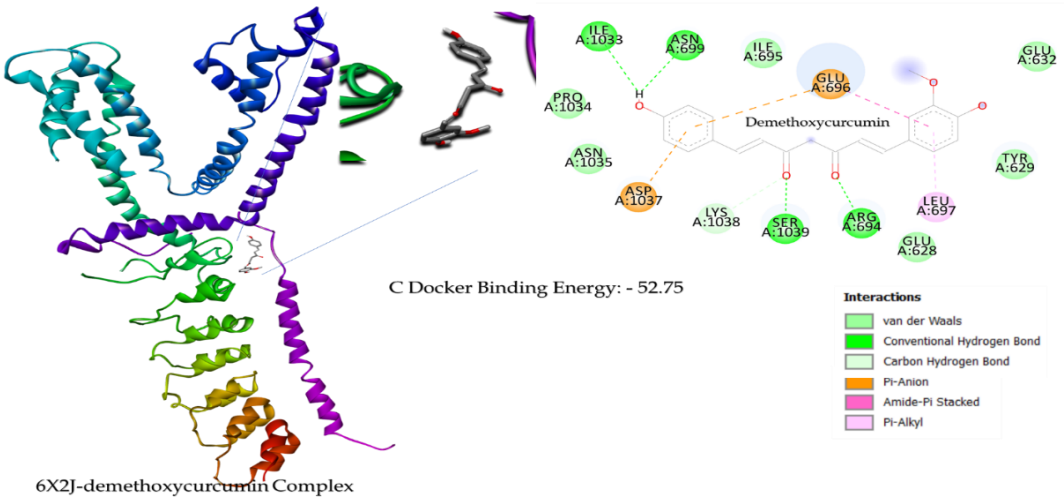

Figure 2: Binding Energy and 2D Binding site analysis of 6X2J and Demethoxyurcumin complex

The docking results shown in Figure 2 illustrate the interaction of Demethoxycurcumin with a target protein, analyzed using the CDOCKER protocol. The image provides both a 3D representation of the protein-ligand complex and a 2D interaction map, highlighting key interactions that contribute to ligand binding.

The left side of the image displays the protein in a ribbon model, with Demethoxycurcumin bound within the receptor cavity. The ligand is depicted in a stick model, positioned in the active site, interacting with the surrounding amino acid residues. The right side of the image presents a 2D schematic of the Demethoxycurcumin binding interactions, with amino acid residues labeled and color-coded based on interaction types. Several residues, including ILE A:1033, PRO A:1034, ASN A:1035, and ILE A:695, form van der Waals interactions, stabilizing the ligand within the binding site. Hydrogen bonds are observed with ASP A:1037 and SER A:1039, playing a crucial role in ligand stabilization and binding affinity. A carbon hydrogen bond interaction is observed with LYS A:1038, contributing to ligand orientation in the receptor cavity. A Pi-Anion interaction is observed with GLU A:696, suggesting electrostatic stabilization between the ligand's aromatic ring and the negatively charged amino acid side chain. An amide-Pi stacking interaction occurs with ARG A:694, further strengthening ligand binding through π-electron interactions. Hydrophobic Pi-Alkyl interactions are formed with LEU A:697, which enhance ligand binding affinity by stabilizing the aromatic ring system.

Similar to Curcumin, Demethoxycurcumin forms strong hydrogen bonding interactions with key active site residues, which contribute to stable binding. The presence of Pi-Anion and Amide-Pi Stacked interactions in Demethoxycurcumin suggests additional electrostatic stabilizations compared to Curcumin, potentially enhancing affinity.

Van der Waals and Pi-Alkyl interactions contribute to the ligand's positioning and stability in both docking studies.

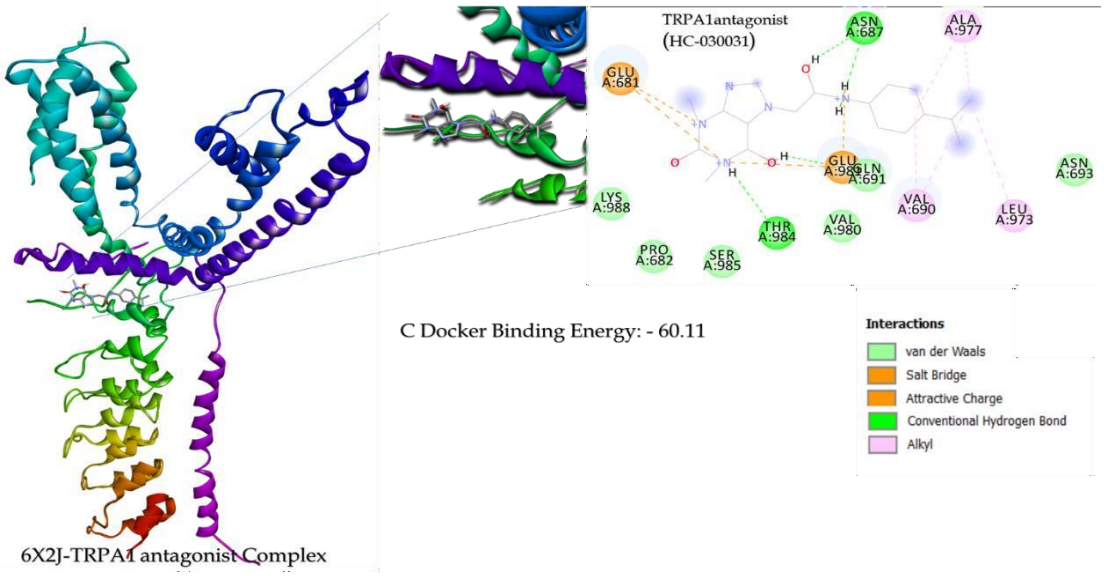

Figure 3: Binding Energy and 2D Binding site analysis of 6X2J and TRPA1 antagonist (HC-030031) complex.

The docking results illustrated in Fig.3 represent the binding interaction of the TRPA1 antagonist (HC-030031) with the TRPA1 receptor (PDB ID: 6X2J) using the CDOCKER protocol. The image contains both 3D and 2D representations, detailing key interactions between the ligand and receptor residues.

The left side of the image shows the TRPA1 receptor in a ribbon model with the antagonist HC-030031 docked into the active site. The ligand is depicted in a stick model, and the docking site is highlighted, showing how the ligand is positioned within the receptor's binding pocket.

The right side of the image presents a 2D schematic of HC-030031's binding interactions, illustrating different types of molecular forces stabilizing the ligand in the active site. Residues such as PRO A:682, SER A:985, THR A:984, VAL A:980, and ASN A:687 participate in van der Waals interactions, which help to maintain ligand stability within the binding pocket. A significant salt bridge interaction is observed with GLU A:681, indicating strong electrostatic attraction between the negatively charged receptor residue and a positively charged region of the ligand. GLU A:681 and GLN A:691 also engage in attractive charge interactions with the ligand, suggesting a potential role in stabilizing the ligand via electrostatic interactions. Hydrogen bonds are observed with ASN A:687 and GLN A:691, which likely contribute to ligand specificity and binding affinity. Hydrophobic alkyl interactions with residues LEU A:973, VAL A:690, and ALA A:977 help stabilize the ligand through hydrophobic interactions, enhancing the overall binding affinity. Unlike Curcumin and Demethoxycurcumin, which relied more on π interactions (Pi-Anion, Pi-Alkyl, and Amide-Pi Stacking), HC-030031 shows a stronger dependency on electrostatic forces (salt bridge and attractive charge interactions), which suggests it may have a different binding mechanism. The presence of strong salt bridge and attractive charge interactions suggests that HC-030031 binds more tightly to the receptor through ionic interactions compared to the previous ligands. Hydrogen bonding and van der Waals forces are common features across all docking studies, indicating their general importance in ligand binding.

The docking results indicate that HC-030031 interacts with TRPA1 through a combination of salt bridge interactions, attractive charge forces, hydrogen bonding, van der Waals, and alkyl interactions.

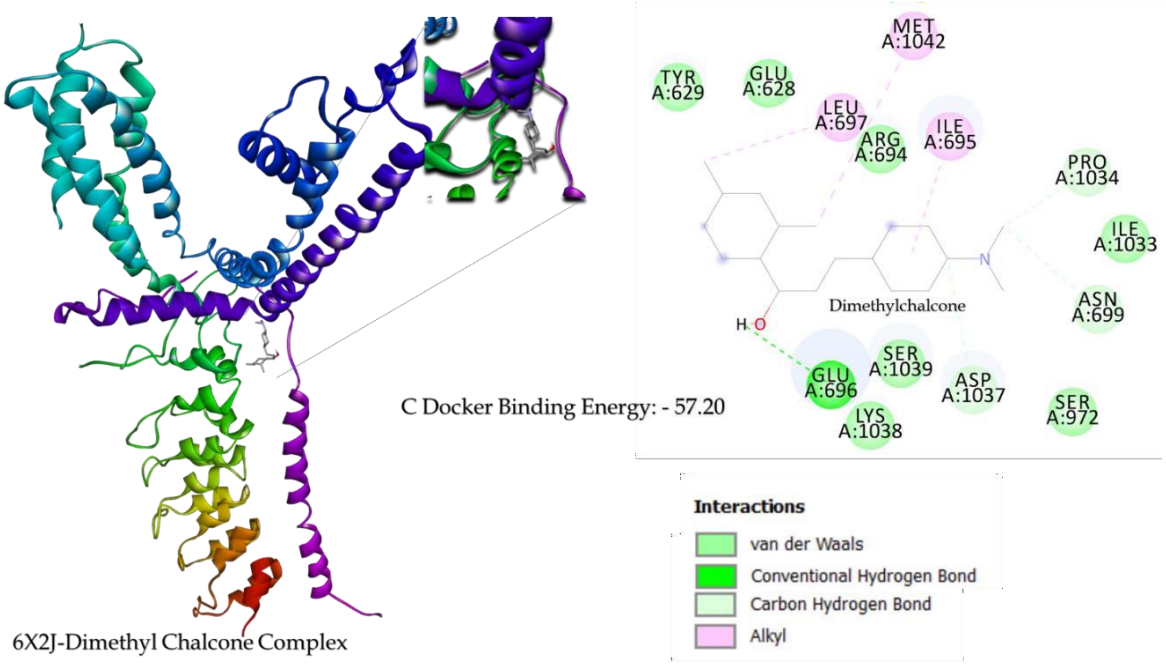

Figure 4: Binding Energy and 2D Binding site analysis of 6X2J and Dimethyl Chalcone complex.

The image represents the molecular docking study of Dimethylchalcone with the TRPA1 receptor, visualized using 3D and 2D interaction diagrams. The docking results provide insights into the binding interactions and stability of Dimethylchalcone within the active site of TRPA1. The TRPA1 receptor (PDB ID: 6X2J) is shown in a ribbon model with a color gradient from blue to red, representing different domains of the protein. Dimethylchalcone is represented as a stick model within the binding pocket, demonstrating its spatial positioning inside the receptor. The 2D interaction diagram on the right side of the image illustrates various binding interactions between Dimethylchalcone and key amino acid residues in the TRPA1 receptor active site.

Several residues, including TYR A:629, GLU A:628, LEU A:697, ARG A:694, ASN A:699, PRO A:1034, ILE A:1033, ASP A:1037, SER A:972, and SER A:1039, exhibit van der Waals interactions, which help stabilize the ligand in the binding pocket. A strong hydrogen bond interaction is observed between Dimethylchalcone and GLU A:696, which contributes significantly to binding affinity and ligand stability. A carbon hydrogen bond interaction is observed with LYS

A:1038, further strengthening the ligand's interaction with the receptor. Hydrophobic alkyl interactions are seen with ILE A:695, MET A:1042, and LEU A:697, indicating the role of hydrophobic interactions in enhancing ligand stability. The presence of a hydrogen bond with GLU A:696 enhances stability, while alkyl and van der Waals interactions contribute to maintaining the ligand within the binding pocket.

MD Simulations results for the protein and ligand structures

The RMSDs of the TRPA1 protein (6X2J), TRPA1 antagonist and Curcumin-TRPA1 protein complexes, measured over a 100 and 300ns period, were found to be 0.56, 0.61, 0.58 nm. These values indicate that there was little structural change in the protein complexes during the simulation. (Fig.5.). The RMSD plot from the MD simulation shows an initial rapid increase in RMSD during the first 0–10 ns, indicating that the system is moving away from its starting structure as it equilibrates. After approximately 10–20 ns, the RMSD stabilizes around 0.4–0.6 nm, with minor fluctuations but no significant rise, suggesting that the system has reached equilibrium and remains structurally stable throughout the simulation. A stable RMSD indicates that the protein or biomolecule maintains its overall structure over time, whereas a continuously increasing RMSD might suggest unfolding or instability.[13]

These RMSD results represent the relative stability of compound complexes throughout the simulation. Overall, the RMSD results indicate that the protein complexes considered were relatively stable throughout the simulation.

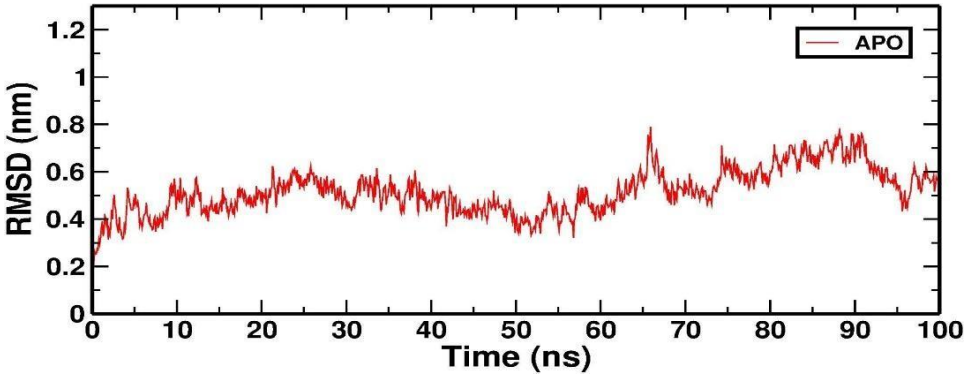

Figure 5: Root means square deviation (RMSD) of backbone atoms of TRPA1 protein (6X2J).

The RMSD plot (Fig.6) shows an initial rapid increase in the first 0–10 ns, indicating that the structure is adjusting from its initial conformation as it equilibrates. After approximately 10–20 ns, the RMSD stabilizes around 0.4–0.6 nm, with small fluctuations. However, between 70–90 ns, the RMSD rises significantly, peaking above 0.8 nm, suggesting possible conformational changes or structural flexibility. Despite these fluctuations, the RMSD does not exhibit an uncontrolled increase, indicating that the system remains relatively stable but undergoes notable deviations compared to its initial structure. The observed fluctuations and peak at around 70–90 ns imply potential conformational changes, flexibility, or interactions that may influence system stability. Compared to the TRPA1(6X2J) system (ligand-free state), this system exhibits greater deviations, which could be due to ligand binding effects. The ligand-bound system, shows increased RMSD may indicate an induced fit mechanism, conformational rearrangement, or partial destabilization.[13]

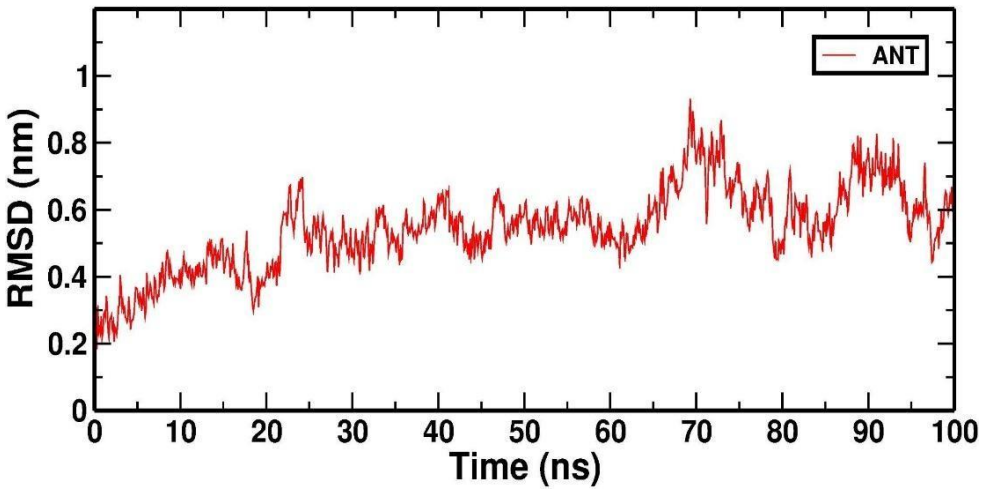

Figure 6: Root means square deviation (RMSD) of backbone atoms of TRPA1 antagonist.

The RMSD plot for Curcumin (Fig.7.) reveals three distinct phases: an initial rise from 0–50 ns, indicating structural

adaptation; major fluctuations between 50–150 ns, with a peak above 0.8 nm around 120–140 ns, suggesting ligand-induced flexibility or structural rearrangement; and stabilization after 150 ns, where RMSD decreases and remains steady around 0.4–0.5 nm, indicating equilibrium. The extended 300 ns simulation was necessary as the system did not stabilize within 100 ns, highlighting the need for longer simulations for certain ligand-bound complexes. The observed peak suggests a significant conformational transition, likely due to induced fit or ligand binding effects. Ultimately, the system stabilizes, and comparing this RMSD with other systems (e.g., TRPA1 or TRPA1 antagonist provides insights into ligand-induced structural stability over extended timeframes.

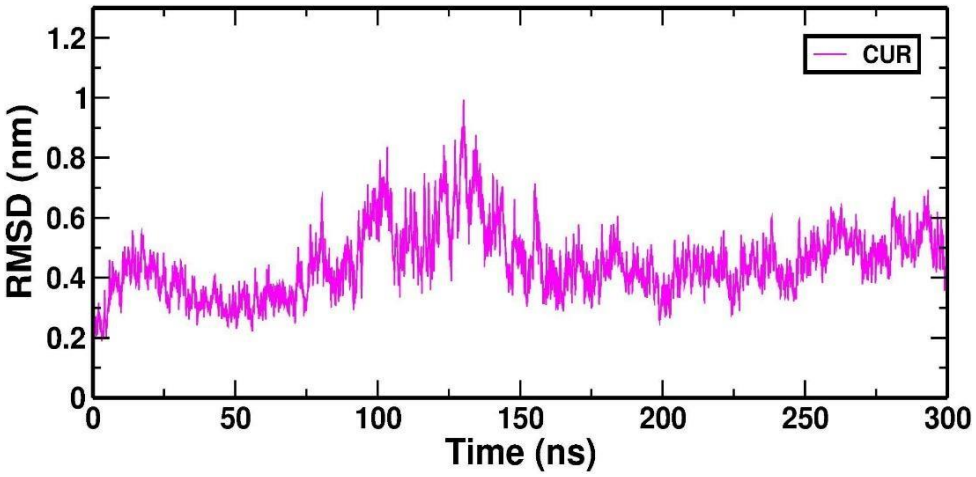

Figure 7: Root means square deviation of backbone atoms of Curcumin.

The RMSF plot (Fig.8.) represents residue-wise flexibility analysis from an Molecular Dynamics (MD) simulation of the TRPA1 system (ligand-free state). RMSF measures atomic fluctuations over time, helping identify flexible and rigid regions in the protein.

Most residues exhibit low RMSF values (below 0.3 nm), indicating overall structural stability.[13] Core secondary structure elements (α-helices and β-sheets) are generally more rigid. Significant peaks around residues 250–320 and 450, indicating high flexibility in these regions. The largest peak near residue 300 suggests a loop or disordered region with substantial motion. The spike around residue 450 could correspond to a terminal or loop region, which is naturally more flexible. Flexible regions often correspond to loops, termini, or binding sites that facilitate conformational changes. The high flexibility near residue 300 suggests potential functional importance, possibly a binding site or interaction region. Comparing this to other systems (e.g., holo or ligand-bound structures) helps assess how ligand binding affects protein flexibility.

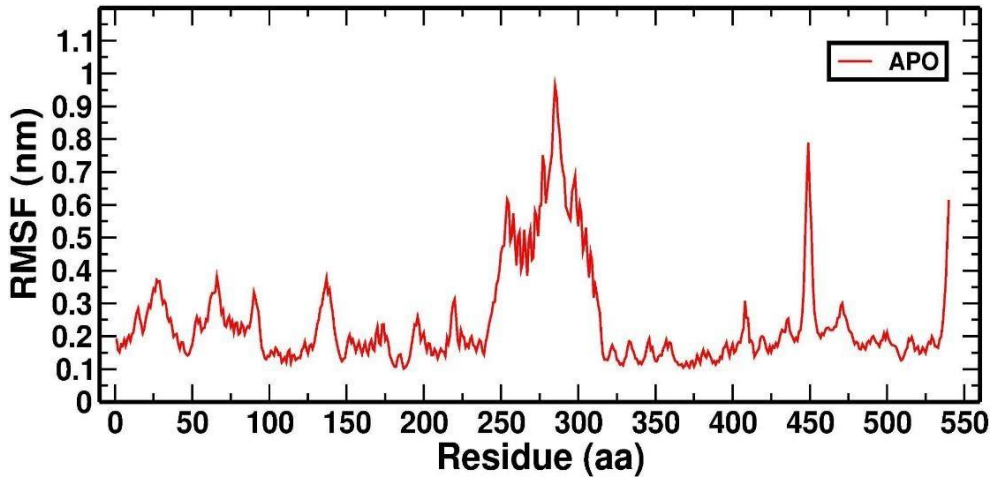

Figure 8: Root means square fluctuation of c-alpha atoms of TRPA1

The RMSF plot (Fig.9) represents the residue-wise flexibility analysis from an MD simulation of the ANT system (ligand-bound state). RMSF quantifies atomic fluctuations over time, highlighting flexible and rigid regions within the protein. Similar to the TRPA1 system, most residues exhibit low RMSF values (below 0.3 nm), indicating overall structural stability. Core secondary structure elements (α-helices and β-sheets) remain relatively rigid.

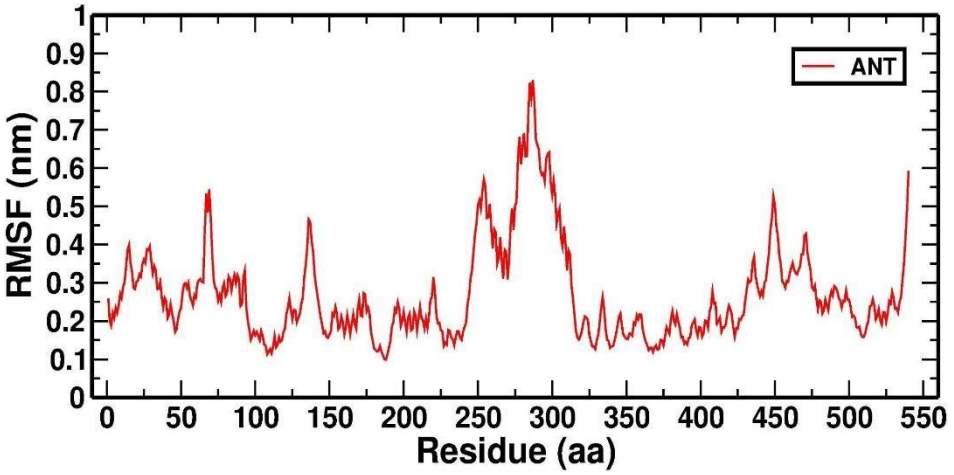

Figure 9: Root means square fluctuation of c-alpha atoms of TRPA1 antagonist

The highest peak appears around residue 300, indicating significant flexibility in this region. Similar peaks are present at residue 250–320 and near the C-terminal (~550 residues), comparable to the TRPA1(APO) system. However, fluctuations in the ANT system are slightly lower than in the APO system, suggesting that ligand binding provides some structural stabilization. The binding of the antagonist appears to slightly reduce flexibility, particularly in functionally important regions. The highest fluctuation (~residue 300) suggests a loop or binding site undergoing conformational adaptation upon ligand interaction.[13]

As shown in Fig.10, the majority of residues exhibit low RMSF values (below 0.3 nm), indicating that these regions are structurally stable. These regions likely correspond to α-helices and β-sheets, which tend to remain rigid throughout the simulation. Notable fluctuations are observed around residue 250–320 and 450–500, similar to the TRPA1 and TRPA1 antagonist systems. A distinct RMSF peak around residue 300 suggests that this region undergoes significant motion, potentially corresponding to a loop or binding site. Additionally, the RMSF peak at residue 450 is more pronounced, indicating increased flexibility in this region compared to the TRPA1 antagonist-bound system. Compared to the TRPA1(APO) system, the overall fluctuations appear slightly reduced, suggesting that ligand binding stabilizes some regions of the protein. However, compared to the TRPA1 antagonist bound system, the curcumin-bound system exhibits slightly higher flexibility in certain regions, indicating that curcumin might not stabilize the protein as effectively as TRPA 1 antagonist.

The RMSF peak near residue 300 is present in all three cases (TRPA1, TRPA1 antagonist, and Curcumin), confirming its functional significance—possibly a binding site or a flexible loop involved in conformational changes.

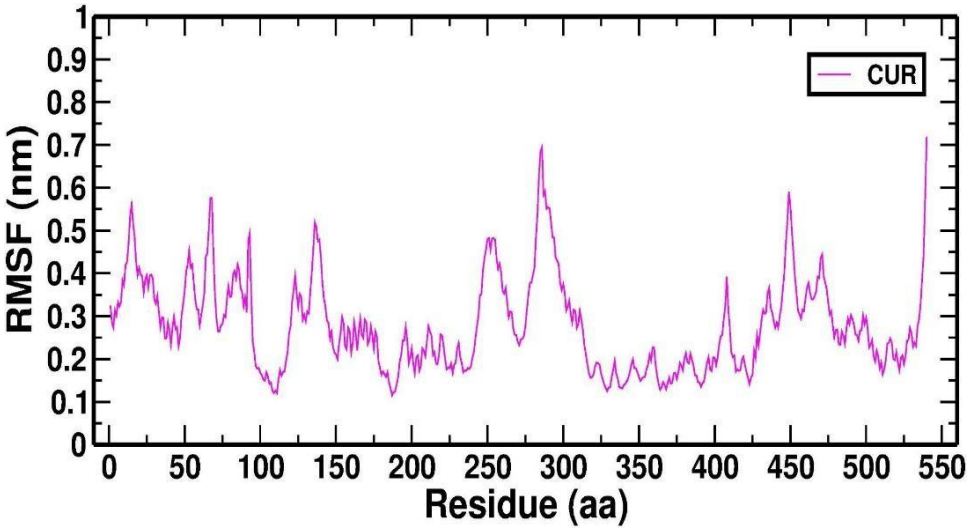

Figure 10: Root means square fluctuation of c-alpha atoms of CUR

The RMSD (Root Mean Square Deviation) plot, as shown in Fig. 11, for 2',4'-dimethyl-4-(dimethylamino) chalcone provides critical insights into its structural stability and conformational changes during molecular dynamics (MD) simulation. Initially, the RMSD exhibits a sharp rise, reflecting the equilibration phase where the system undergoes structural adjustments to adapt to the simulation environment. This phase is essential as it captures the molecular reorganization from its starting conformation to a more energetically favorable and stable binding mode.

As the simulation progresses, the RMSD stabilizes with only minor fluctuations, indicating that the system has reached a relatively steady state. This suggests that while the chalcone maintains structural integrity within the binding site, it still retains a degree of conformational flexibility necessary for dynamic interactions with its environment. The minor deviations observed throughout the simulation likely correspond to natural thermal motions, small-scale rearrangements, or transient interactions with surrounding residues or solvent molecules.

The overall RMSD trend signifies that 2',4'-dimethyl-4-(dimethylamino) chalcone exhibits stability within the simulation time frame, with no signs of drastic structural disruptions or unfolding. This behaviour is crucial for its potential as a bioactive molecule, as maintaining structural stability while allowing necessary flexibility can enhance its binding efficiency and molecular recognition in a biological system. The RMSD data thus reinforces the molecule's suitability for further computational and experimental validation in drug design studies.

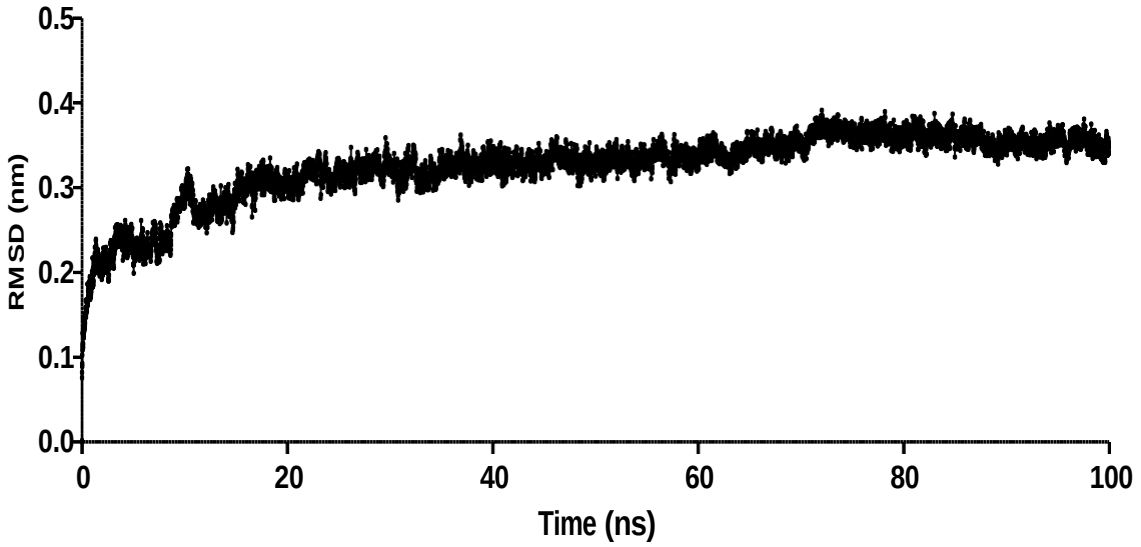

Figure 11: Root means square deviation (RMSD) of backbone atoms of 2',4'-dimethyl-4-(dimethylamino) chalcone.

If significant deviations occur, they may indicate conformational changes, possible structural instability, or ligand-induced flexibility. The final phase shows whether the molecule attains a stable conformation or continues to fluctuate. A steady RMSD suggests strong ligand binding and stability, whereas persistent fluctuations may imply weak interactions or ligand detachment.

The radius of gyration (Rg) is a measure of the compactness of a protein's structure, which can be calculated as the mass-weighted average distance of atoms from the protein's center of mass. The Rg plot can be used to visualize how the overall shape and folding of the protein changes over time during a molecular dynamics simulation. The Rg plot in Figure 12 illustrates the changes in the protein's structure at different time points during the simulation trajectory. The Radius of Gyration (Rg) plot represents the structural compactness of the APO (ligand-free) system during a 100 ns molecular dynamics (MD) simulation. The Rg value quantifies the distribution of atomic positions relative to the center of mass, indicating protein folding or unfolding over time.

Initial Phase (0–10 ns): The Rg starts at around 3.3 nm and quickly stabilizes, suggesting an initial structural relaxation as the protein adapts to the simulation environment. Stable Region (10–100 ns): The Rg fluctuates around 3.4 nm, indicating that the protein maintains a relatively compact structure throughout the simulation. Minor variations suggest natural breathing motions without significant unfolding or collapse. Minor Fluctuations (~60–80 ns): A slight increase in Rg is observed, possibly due to transient conformational changes or loop flexibility. However, the structure returns to a stable state, implying that no major unfolding occurs.

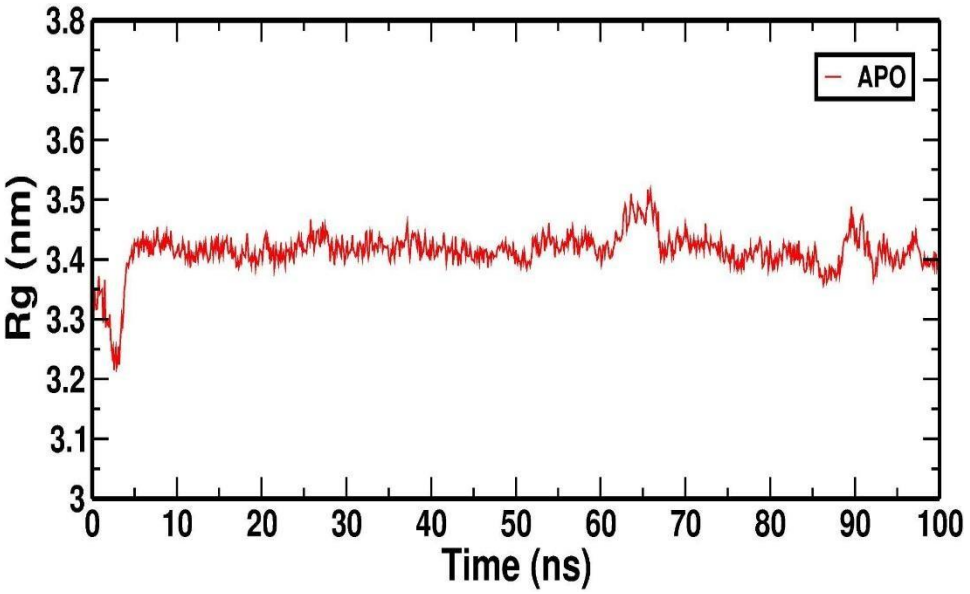

Figure 12: Radius of Gyration (RG) of backbone atoms of with TRPA1

As shown in the Fig.13 the protein starts in a compact conformation (~3.3 nm at 0 ns). Small fluctuations are observed between 3.3–3.5 nm: The system remains relatively stable, with minor fluctuations. Gradual increase in Rg (~3.4–3.6 nm from 20–100 ns) suggests minor structural expansion over the simulation. Despite fluctuations, the Rg remains within a narrow range (3.3–3.6 nm), indicating no major unfolding or collapse of the protein structure. A stable Rg profile (~3.3–3.6 nm) suggests that the protein maintains its structural integrity throughout the simulation. Small fluctuations are expected due to natural protein flexibility. No drastic changes indicate that the ligand does not significantly destabilize the protein. If the Rg had drastically increased (e.g., >4.0 nm), it could indicate protein unfolding or destabilization, but this is not observed here. The protein-ligand complex remains stable over 100 ns, with only minor structural adjustments. The antagonist (ANT) does not significantly alter the protein's compactness, making it a potentially stable binding candidate.

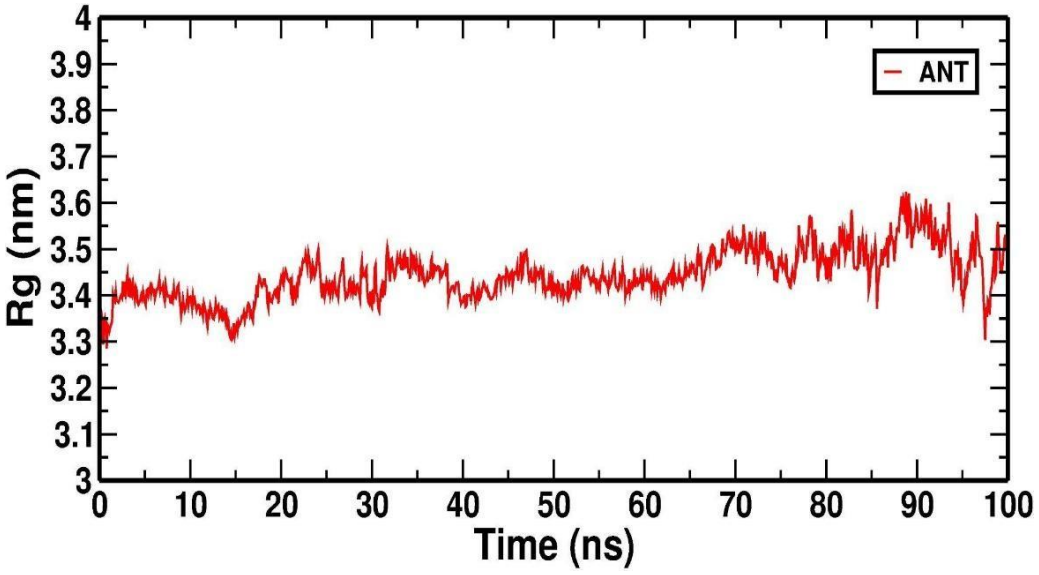

Figure 13: RG of backbone atoms of with TRPA1 antagonist (ANT)

The radius of gyration (Rg) analysis provides insights into the structural stability of the protein-ligand complex during the 300 ns molecular dynamics simulation as shown in Fig.14. Initially, the Rg value as shown in Fig.14, is observed in the range of 3.3–3.4 nm, indicating that the system starts in a compact conformation. Around 50 ns, a minor decrease to approximately 3.2 nm suggests an initial relaxation phase of the protein. This is followed by an increase in Rg between 50–150 ns, fluctuating between 3.4–3.6 nm, which may indicate structural expansion and conformational flexibility due to

ligand binding interactions. After 200 ns, the Rg stabilizes within the range of 3.3–3.4 nm, suggesting that the system reaches equilibrium and maintains a stable protein-ligand interaction.

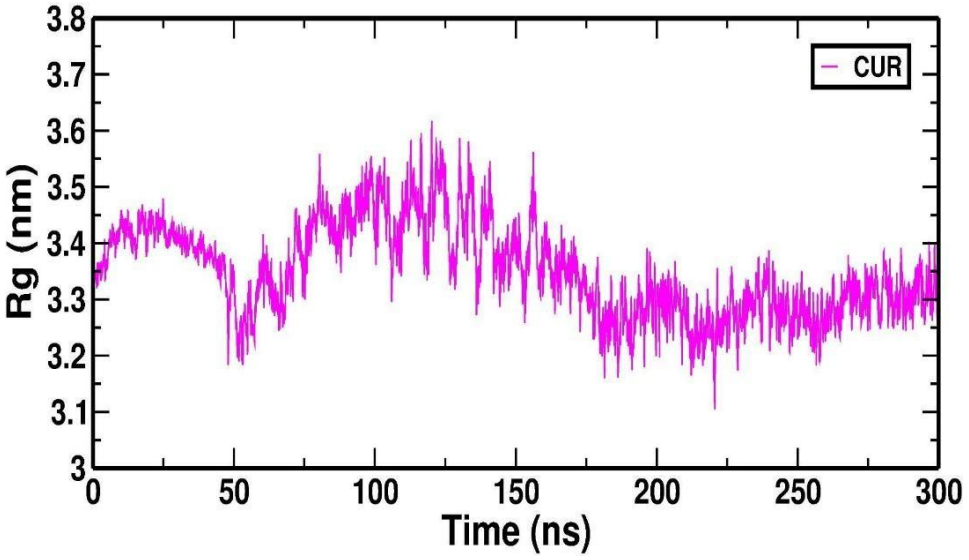

Figure 14: RG of backbone atoms of with CUR

Throughout the simulation, the Rg remains within a narrow range of 3.2–3.6 nm, signifying that no major unfolding or structural collapse occurs. The fluctuations observed between 50–150 ns could be attributed to protein-ligand binding adjustments or conformational flexibility, allowing the system to adapt dynamically.

Importantly, after 200 ns, the system achieves stability, indicating that curcumin (CUR) does not disrupt the protein's compactness but rather supports some degree of conformational adaptability. The absence of significant unfolding or collapse further indicates a strong and favourable interaction between CUR and the protein.

Hydrogen Bond (H-bond) Analysis

The stability of protein-ligand complexes can be attributed to the formation of hydrogen bonds between the protein and the ligand. In this research, the hydrogen bonds that were identified through molecular docking analysis were further confirmed through simulation analysis. The hydrogen bond (H-bond) analysis provides crucial insights into the stability and interaction strength of protein-ligand complexes during molecular dynamics simulations. The number of hydrogen bonds formed between the protein and the ligand is a key determinant of binding stability and affinity. The hydrogen bond formation for Curcumin, Demethoxycurcumin, TRPA1 antagonist and Dimethyl Chalcone is shown in Fig.15.

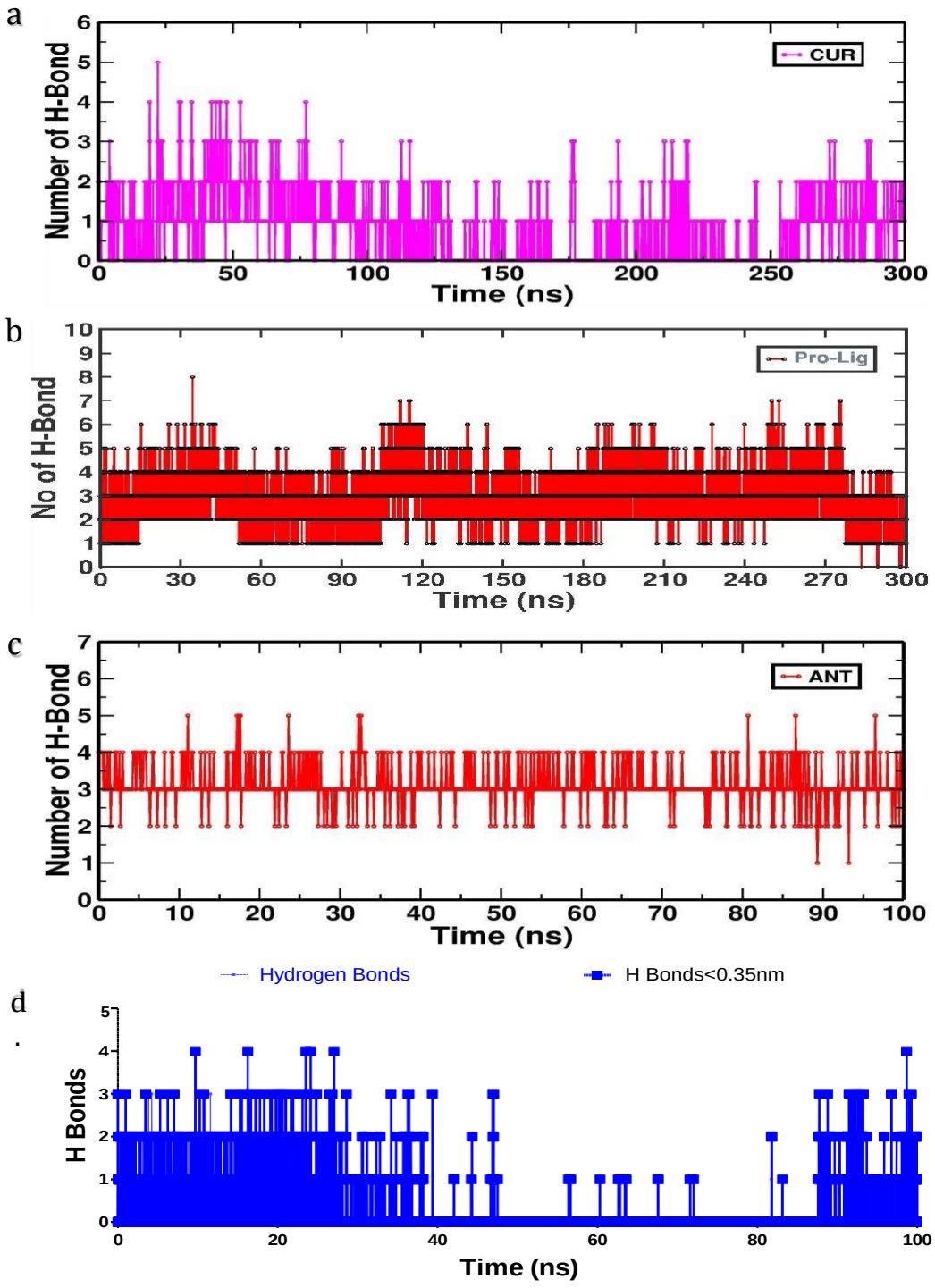

Figure 15: Hydrogen Bond formed during MD Simulation. a. Curcumin, b. Demethoxy Curcumin, c. TRPA1 antagonist, d. Dimethyl Chalcone

In the Curcumin system, as shown in Fig. 15(a) the number of hydrogen bonds fluctuates between 1 and 4 throughout the 300 ns simulation, indicating a moderate interaction with the protein. The bond formation appears transient, suggesting that curcumin binds dynamically, with occasional loss and reformation of hydrogen bonds. This may imply that curcumin interacts flexibly with the protein without rigid constraints, which could be beneficial for reversible binding.

For the Demethoxy curcumin, as shown in Fig. 15(b) a higher and more stable hydrogen bonding pattern is observed, ranging between 2 and 8 bonds during the simulation. The presence of multiple persistent hydrogen bonds suggests a strong

and stable interaction between the protein and the ligand. Notably, the dimethoxy curcumin maintains at least 3-4 hydrogen bonds consistently, demonstrating its strong affinity and structural stability throughout the simulation period.

The TRPA1 antagonist as shown in Fig. 15(c) shows a relatively stable hydrogen bond pattern, with bonds ranging between 2 and 6, maintaining an average of 3-4 hydrogen bonds. This indicates that the antagonist forms a reliable interaction with the protein, similar to dimethoxy curcumin, but with slightly fewer fluctuations.

The Dimethyl chalcone hydrogen bonding pattern is shown in Fig.15(d). During the early phase (0–40 ns), the number of hydrogen bonds fluctuates between 1 and 4, indicating an initially stable interaction between the protein and ligand. In the mid-phase (40–80 ns), a noticeable decline in hydrogen bonds is observed, with some time intervals showing no bonds at all, suggesting a temporary loss of interaction due to ligand movement or conformational changes in the protein. However, in the late phase (80–100 ns), the hydrogen bonds reappear, fluctuating between 1 and 4, indicating that the ligand may have reoriented or stabilized within the binding pocket.

The hydrogen bond analysis confirms that Dimethyl chalcone, Demetoxycurcumin and TRPA1 antagonist exhibit stronger and more stable interactions compared to curcumin, which shows dynamic but weaker hydrogen bonding behaviour.

Results of In-vivo Chronic Constriction Injury animal model for neuropathic pain for evaluating Curcumin, and (E)-3-(4-(dimethylamino)phenyl)-1-(2,4-dimethylphenyl)prop-2-en-1-one

Based on the above MD simulation studies and Molecular docking studies Curcumin and Dimethyl Chalcone [(E)-3-(4-(dimethylamino)phenyl)-1-(2,4-dimethylphenyl)prop-2-en-1-one] were selected for in-vivo studies in Chronic Constriction injury animal model of neuropathic pain.

The presented bar graph (see Fig.16.) shows the percentage reversal of paw withdrawal (hyperalgesia) following the administration of different doses of curcumin, a TRPA1 antagonist, and pregabalin in rats subjected to the Chronic Constriction Injury (CCI) model.

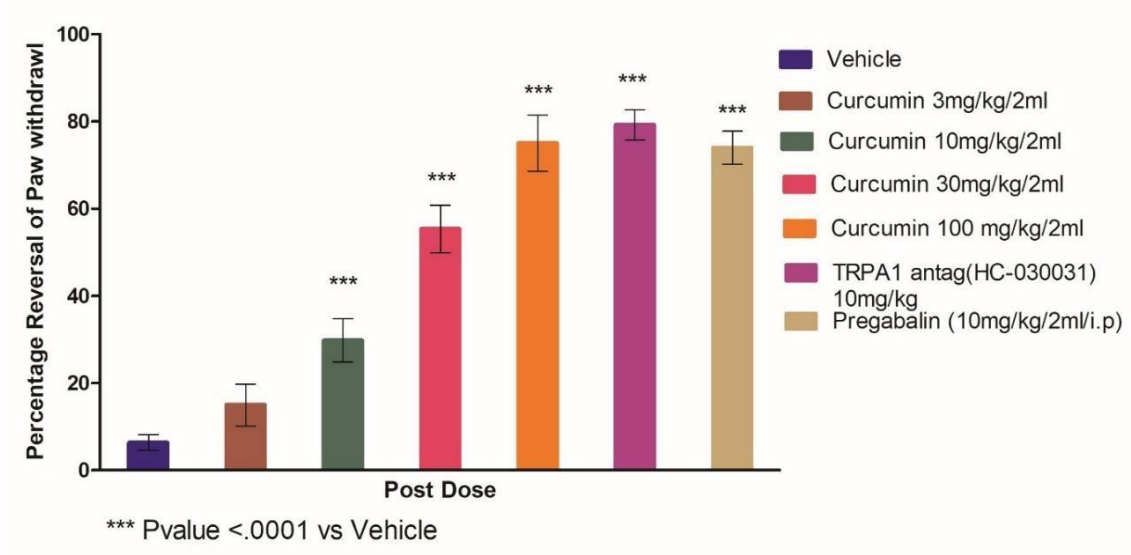

Figure 16: Effect of Curcumin on Neuropathic Pain in the Chronic Constriction Injury (CCI) animal model.

The percentage reversal of paw withdrawal was assessed using the Randall-Selitto test at 3 hours post-dosing. Data represent mean ± SEM (n = 6). Statistical significance was determined against the vehicle group (***P < 0.0001). Higher doses of Curcumin and TRPA1 antagonist (HC-030031) showed significant efficacy comparable to Pregabalin.

The Vehicle Group (Blue Bar) shows minimal reversal of hyperalgesia, indicating that untreated CCI rats experience persistent neuropathic pain. Curcumin 3 mg/kg (Red Bar): Shows a modest reversal of paw withdrawal (14.98%), suggesting partial but limited analgesic efficacy at this low dose. Curcumin 10 mg/kg (Green Bar) demonstrates a significant improvement (29.75%), indicating better pain alleviation. Curcumin 30 mg/kg (Pink Bar) further enhances the percentage reversal (55.3%), showing a strong dose-dependent effect. Curcumin 100 mg/kg (Orange Bar) exhibits the highest efficacy among curcumin-treated groups (~75.01%), suggesting an optimal dose for neuropathic pain relief. TRPA1 Antagonist (Purple Bar, HC-030031 10 mg/kg) shows a comparable effect (79.16%) to the highest dose of curcumin, indicating a strong analgesic effect via TRPA1 inhibition. Pregabalin (Brown Bar, 10 mg/kg i.p.) also exhibits 73.95% reversal, reinforcing its effectiveness as a standard treatment for neuropathic pain.

Curcumin exhibits a dose-dependent analgesic effect in the CCI model, with the 100 mg/kg dose providing the highest reversal of hyperalgesia. The TRPA1 antagonist (HC-030031) and pregabalin produce similar or slightly better effects, suggesting that TRPA1 inhibition and calcium channel modulation play a key role in pain relief.

These results highlight curcumin's potential as a natural therapeutic alternative for neuropathic pain, warranting further investigation into its mechanisms of action and long-term efficacy.

Subsequently, the analgesic effect of Dimethyl Chalcone was evaluated in a Chronic Constriction Injury (CCI) animal model of neuropathic pain as shown in Fig.17. The percentage reversal of paw withdrawal was assessed using the Randall-Selitto test at 3 hours post-dosing, and the efficacy of different doses of Dimethyl Chalcone was compared to a vehicle control, a TRPA1 antagonist (HC-030031), and Pregabalin. The results demonstrated a dose-dependent increase in the analgesic effect of Dimethyl Chalcone, with higher doses showing significant pain relief comparable to the standard drugs.

At lower doses (3 mg/kg and 10 mg/kg), Dimethyl Chalcone exhibited minimal to moderate efficacy in reversing paw withdrawal latency, indicating a partial analgesic response. However, a substantial improvement in pain relief was observed at 30 mg/kg, and the highest dose (100 mg/kg) resulted in a marked increase in analgesic efficacy. The 100 mg/kg dose showed a statistically significant effect (***P < 0.0001) compared to the vehicle-treated group, suggesting that Dimethyl Chalcone at higher concentrations has a strong potential for neuropathic pain management.

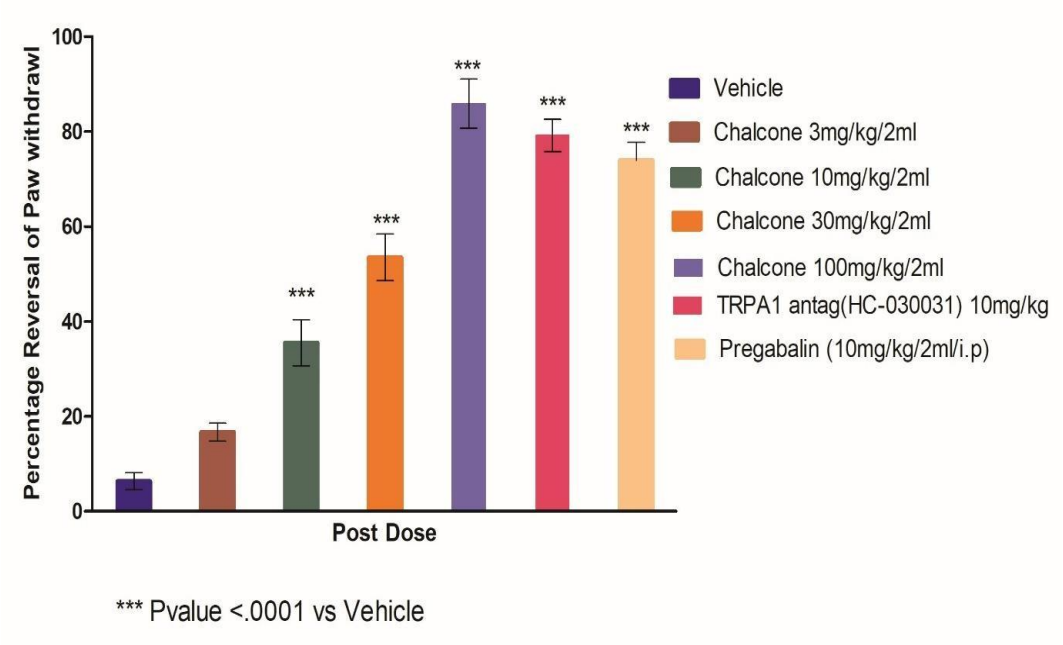

Figure 17: Effect of Dimethyl chalcone in neuropathic pain in the Chronic Constriction Injury (CCI) animal model.

The percentage reversal of paw withdrawal was assessed using the Randall-Selitto test at 3 hours post-dosing. Data represent mean ± SEM (n = 6). Statistical significance was determined against the vehicle group (***P < 0.0001). Higher doses of dimethyl chalcone and TRPA1 antagonist (HC-030031) showed significant efficacy comparable to Pregabalin.

When compared to the reference drugs, the TRPA1 antagonist (HC-030031) and Pregabalin (10 mg/kg), Dimethyl Chalcone at 100 mg/kg exhibited comparable efficacy. Both HC-030031 and Pregabalin significantly reversed paw withdrawal latency, supporting their established roles in neuropathic pain relief. The similarity in efficacy between the highest dose of Dimethyl Chalcone and these standard drugs suggests that Dimethyl Chalcone may exert its analgesic effect through modulation of TRPA1 channels or other pain-related pathways.

The findings highlight the potential of Dimethyl Chalcone as a promising therapeutic candidate for neuropathic pain. Its dose-dependent efficacy suggests that it may serve as an alternative or adjunct to existing neuropathic pain treatments.

Results of Histological Analysis of Sciatic nerve samples

The longitudinal section of the sciatic nerve was subjected for histological analysis for studying the morphological changes in the sciatic nerve for comparison between treated and untreated animals as shown in Fig.18.

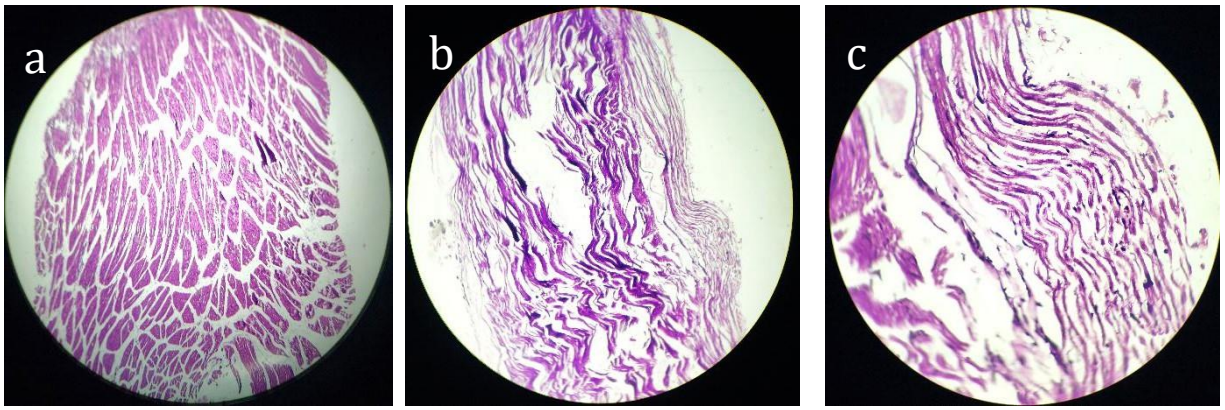

Figure 18: Histological Analysis of Sciatic Nerve in CCI Model (H&E, 40×)

Histological analysis of sciatic nerve sections from the Chronic Constriction Injury (CCI) model. Hematoxylin and eosin (H&E) staining was used to assess nerve morphology (Magnification: 40x). (a) Normal (control) sciatic nerve showing well-organized nerve fibers with intact myelin sheaths and normal architecture. (b) Sciatic nerve from CCI-induced neuropathic pain model showing disrupted nerve fibers, degeneration, and distorted myelin sheaths, indicating nerve injury and pathological changes associated with neuropathy. (c) Sciatic nerve from Pregabalin treated CCI-induced neuropathic pain model showing disorganized and wavy nerve fibers, irregular and fragmented fibres indicating myelin breakdown, presence of dark-stained nuclei suggests immune cell infiltration (macrophages, lymphocytes), leading to inflammation and potential exacerbation of nerve damage. and Increased extracellular matrix deposition and dense connective tissue fibers indicate fibrosis, which can hinder nerve regeneration and lead to chronic neuropathic pain.

Nerve Morphology of the section as shown in Fig.18(a) exhibits a well-organized nerve fiber arrangement with clearly defined fascicles, suggesting preserved structural integrity. The nerve fibers appear aligned, indicating minimal architectural distortion. There is an absence of vacuolated spaces and axonal fragmentation, indicating little to no significant axonal degeneration. The nerve fibers remain relatively intact. The nerve fibers demonstrate a uniform structure, with minimal evidence of myelin breakdown. This suggests that the myelin sheath remains largely intact, supporting efficient nerve conduction. Unlike pathological sections showing chronic constriction injury (CCI)-induced neuropathy, this section does not display substantial infiltration of inflammatory cells. There are no prominent clusters of dark-stained nuclei indicative of immune cell infiltration. The extracellular matrix appears organized with minimal fibrotic deposition. The absence of excessive connective tissue accumulation suggests that there is no significant fibrosis affecting nerve function.

The nerve morphology of the section as shown in Fig.18(b) exhibits disorganized and wavy fibers, which is indicative of potential damage. The parallel alignment of nerve fibers seems to be disrupted, suggesting structural abnormalities. The nerve shows signs of axonal degeneration, evident from the disrupted and irregular fiber arrangements. There may be axonal swelling or vacuolization, which are characteristic of nerve damage in conditions such as chronic constriction injury (CCI)-induced neuropathy. There is a notable loss or disruption of the myelin sheath, as observed from the irregular and fragmented fiber staining patterns. The myelin sheaths appear to be degenerated or thinned, suggesting demyelination, which is common in nerve injury models. Although inflammatory cells (such as macrophages and lymphocytes) may not be distinctly visible in this H&E-stained image, regions with dense staining and cellular debris could indicate the presence of inflammation. This is expected in neuropathic pain models, where chronic nerve injury leads to an immune response. The presence of dense, wavy, and irregularly arranged collagen fibers suggests fibrosis, which occurs due to excessive deposition of extracellular matrix components in response to nerve injury. This fibrosis can contribute to nerve dysfunction and pain by impairing nerve regeneration.

The nerve morphology of the section as shown in Fig.18(c) exhibits disorganized and wavy nerve fibres, suggesting structural alterations often seen in chronic nerve injury. The parallel alignment of the nerve fascicles is disrupted, indicating potential damage and degeneration of the nerve. The image reveals irregular and distorted fibers, which may represent axonal degeneration. Axonal swelling or fragmentation may be present, which is a hallmark of nerve damage in neuropathic conditions. There is evidence of myelin sheath disruption, seen as an irregular and fragmented fiber pattern. Loss or thinning of myelin sheaths can impair nerve signal conduction and contribute to neuropathic pain. The waviness and separation of fibers suggest possible demyelination or myelin breakdown. The presence of dark-stained nuclei scattered among the fibers may indicate infiltration of immune cells, such as macrophages and lymphocytes, which are typically

involved in nerve inflammation following injury. This inflammatory response can exacerbate nerve damage and contribute to pain hypersensitivity. There appears to be an increase in extracellular matrix deposition, indicated by dense, irregular connective tissue fibers. This suggests fibrotic changes, which are common in chronic nerve injury models, such as the chronic constriction injury (CCI) model. Fibrosis can hinder nerve regeneration and lead to persistent neuropathic pain.

4. CONCLUSION

The findings from this study provide strong evidence supporting the potential of Curcumin and Dimethyl Chalcone as effective therapeutic candidates for neuropathic pain management. The docking analysis showed Dimethyl chalcone (-57.20; C Docker) with the highest binding affinity and the MD simulations data validated the docking results. The in-vivo results from the Chronic Constriction Injury (CCI) animal model demonstrate a significant, dose-dependent analgesic effect of both compounds, with higher doses (100 mg/kg) exhibiting pain relief comparable to standard treatments like Pregabalin and the TRPA1 antagonist (HC-030031). Histological analysis of sciatic nerve samples further confirmed that untreated CCI-induced neuropathy led to severe structural damage, demyelination, and inflammation, while treatment with Curcumin and Dimethyl Chalcone attenuated nerve degeneration and improved nerve integrity. The observed efficacy suggests that these compounds may exert their effects by modulating TRPA1 receptor activity and other pain-related pathways. Overall, these results highlight Dimethyl Chalcone as promising synthetic therapeutic agent for neuropathic pain.

5. ACKNOWLEDGEMENT

I would like to acknowledge the management Sri Ramachandra Institute of higher Education and Research and Narasaraopeta Institute of Pharmaceutical Sciences for their continuous support in completing this work.

6. FUNDING

Self

7. CONFLICTS OF INTEREST

There are no conflicts of interest for the above work

REFERENCES

[1] Meents JE, Ciotu CI, Fischer MJ. TRPA1: a molecular view. J Neurophysiol. 2019; 121: 427-443.

[2] Fernandes E, Fernandes M, Keeble J. The functions of TRPA1 and TRPV1: moving away from sensory nerves. Br J Pharmacol. 2012; 166: 510-521.

[3] Viana F. TRPA1 channels: molecular sentinels of cellular stress and tissue damage. J Physiol. 2016; 594: 4151-4169.

[4] Cao B, Xu Q, Shi Y, Zhao R, Li H, Zheng J, Liu F, Wan Y, Wei B. Pathology of pain and its implications for therapeutic interventions. Sig Transduct Target Ther. 2024; 9: 155.

[5] Yao K, Dou B, Zhang Y, Chen Z, Li Y, Fan Z, Ma Y, Du S, Wang J, Xu Z. Inflammation—the role of TRPA1 channel. Front Physiol. 2023; 14: 1093925.

[6] Bautista DM, Pellegrino M, Tsunozaki M. TRPA1: A gatekeeper for inflammation. Annu Rev Physiol. 2013; 75: 181-200.

[7] Stucky CL, Dubin AE, Jeske NA, Malin SA, McKemy DD, Story GM. Roles of transient receptor potential channels in pain. Brain Res Rev. 2009; 60: 2-23.

[8] Souza Monteiro de Araujo D, Nassini R, Geppetti P, De Logu F. TRPA1 as a therapeutic target for nociceptive pain. Expert Opin Ther Targets. 2020; 24: 997-1008.

[9] Nilius B, Appendino G, Owsianik G. The transient receptor potential channel TRPA1: from gene to pathophysiology. Pflugers Arch. 2012; 464: 425-458.

[10] Hoffstaetter LJ, Bagriantsev SN, Gracheva EO. TRPs et al.: a molecular toolkit for thermosensory adaptations. Pflugers Arch. 2018; 470: 745-759.

[11] Zhong S, Hou Y, Zhang Z, Guo Z, Yang W, Dou G, Lv X, Wang X, Ge J, Wu B. Identification of novel natural inhibitors targeting AKT Serine/Threonine Kinase 1 (AKT1) by computational study. Bioeng. 2022; 13: 12003-12020.

[12] Ferrari IV, Patrizio P. Development and validation molecular docking analysis of human serum albumin (HSA). BioRxiv. 2021; 2021-07.

[13] Pronk S, Páll S, Schulz R, Larsson P, Bjelkmar P, Apostolov R, Shirts MR, Smith JC, Kasson PM, Van Der Spoel D. GROMACS 4.5: a high-throughput and highly parallel open source molecular simulation toolkit.

Bioinformatics. 2013; 29: 845-854.

[14] Abraham MJ, Gready JE. Optimization of parameters for molecular dynamics simulation using smooth particle-mesh Ewald in GROMACS 4.5. J Comput Chem. 2011; 32: 2031-2040.

[15] Bennett GJ, Xie YK. A peripheral mononeuropathy in rat that produces disorders of pain sensation like those seen in man. J Pain. 1988; 33: 87-107.

[16] Kalichman MW, Powell H, Myers R. Quantitative histologic analysis of local anesthetic-induced injury to rat sciatic nerve. J Pharmacol Exp Ther. 1989; 250: 406-413